Research Square

Preprints are preliminary reports that have not undergone peer review.
They should not be considered conclusive, used to inform clinical practice,
or referenced by the media as validated information.

Influence of Hydrogeomorphic Variability on Physicochemical and Biological Conditions in the Water Column of a Tropical Alluvial Zone

MIGUEL ANGEL SALCEDO MEZA
Universidad Juárez Autónoma de Tabasco https://orcid.org/0000-0003-4117-0770
Alberto J. Sánchez
alberthoj.sanchez@gmail.com
Universidad Juárez Autónoma de Tabasco https://orcid.org/0000-0002-9967-6494
Allan Keith Cruz-Ramírez
Universidad Juárez Autónoma de Tabasco https://orcid.org/0000-0002-6413-2200
Rosa Florido
Universidad Juárez Autónoma de Tabasco https://orcid.org/0000-0001-9796-6052
Nicolás Álvarez-Pliego
Universidad Juárez Autónoma de Tabasco https://orcid.org/0000-0001-5824-8410

Research Article

Keywords: Indicators, distribution patterns, physicochemical processes, lateral interconnectivity, riverine wetland

Posted Date: November 2nd, 2026

DOI: https://doi.org/10.21203/rs.3.rs-11566908/v1

License: This work is licensed under a Creative Commons Attribution 4.0 International License. Read Full License

Additional Declarations: The authors declare no competing interests.

Abstract

The variability of 11 physicochemical and biological variables in the water column was analyzed in lentic and lotic environments during two intraannual water level periods over 10 non-consecutive years within a hydraulically interconnected alluvial zone of a tropical fluvial system. The evaluation included the limnological characterization, a principal component analysis (PCA) based on eight key variables, and the examination of inherent and recurrent variability of data through violin plots. The limnological characterization and PCA, both based on variable-level analysis, partially explained the variation among four conditions: lotic high water level, lentic high water level, lotic low water level, and lentic low water level. Whereas, the analysis of inherent data variability pointed out three conditions associated with kinetic energy and water column processes. First, the fluvial explained primarily by sediment transport and nutrient enrichment. Second, lateral homogenization of electric conductivity, water transparency and dissolved oxygen saturation. Third, lentic in low water level, when lakes worked as bioreactors exhibiting high biology productivity and oxygen supersaturation. In conclusion, the inherent data variability of the key variables supports the hypothesis that the physicochemical variability is driven by recurrent and interactive conditions. These findings show that the analysis of data variability provides a useful tool for understanding water column dynamics and identifying the principal conditions regulating the ecological functioning of tropical riverine wetlands.

1. Introduction

The interactions among biochemical processes and biota across geomorphic elements in the longitudinal and lateral dimensions of fluvial systems are markedly determined by surface hydraulic interconnectivity (Ward 1989; Amoros and Bornete 2002; Liu and Wang 2018). This connectivity regulates spatial and temporal variability in physicochemical water conditions and primary production within riverine wetlands (Ward 1989; Shen and Liu 2021; Zheng et al. 2025). In alluvial longitudinal zones, the hydrologic interconnectivity brings about the multidirectional exchange of materials and organisms among the geomorphic elements in the riverine wetlands. These driving forces, together with geomorphic contention factors, lead to multiscale spatiotemporal variability in the transport, production, storage, recycling and release of inorganic and organic matter through the trophic webs linking rivers, channels, and lakes (Tockner et al. 2000; Junk 2002; Covino 2017; Savenko and Savenko 2022; Chaparro et al. 2023; Jeethu and Kaladevi 2025; Zhang 2025).

Under the HLW period, the main river, together with its distributaries and tributaries, increases the transport of inorganic and organic materials, whether suspended or dissolved (Wohl et al. 2021). Moreover, the rise of the water level in the rivers strengthen the horizontal interchange of these inorganic and organic materials, as part of the production and transport processes among rivers, channels and lakes (Ward 1989; Junk 2002; Thomaz et al. 2007; Mayora et al. 2020; McInerney et al. 2020; Park et al. 2022). In HLW, the lateral surface connection between lotic and lentic elements promoted the homogenization of water parameters and aquatic biota, mainly when the hydraulic interconnectivity by geomorphic contention factors almost disappear for the overflowing of lakes and floodplains (Thomaz et al. 2007; Bek et al. 2025). Then, the similar conditions of ions, water transparency and primary production among rivers, and lakes are linked to the water volume, deposition of organic and inorganic matter, and the degradation of the organic fraction by depleting the dissolved oxygen (Diaz and Breitburg 2009; Obolewski et al. 2018; Carhart et al. 2021; Walalite et al. 2023).

In contrast, lakes act as bioreactors during LWL periods, enhancing nutrient transformation and recycling (Wantzen et al. 2008; Marton et al. 2015; Evenson et al. 2018). During this period, lakes are characterized by sediment resuspension, reduced light penetration, and elevated concentrations of nitrogens and phosphorus. These nutrients are rapidly assimilated, supporting enhanced primary production and often leading to high dissolved oxygen saturation in tropical wetlands (Carlson and Havens 2005; Cruz-Ramírez et al. 2019a; Wu et al. 2019; Castillo 2020; Shen and Liu 2021; Salcedo et al. 2022). Despite the reduced water volume, the lateral hydrological connectivity with rivers persists through permanent channels (Shen and Liu 2021), while salt concentrations increases due to evapoconcentration under warmer

and shalower conditions (de Wilde et al. 2015). Concurrently, the attenuation of kinetic energy in the rivers diminishes the suspended solid transport favouring sedimentation and light penetration (Thomaz et al. 2007; Arisanty and Saputra 2017; Lopera-Congote et al. 2020).

As noted above, spatial physicochemical and biological variability under contrasting water-level periods have been extensively documented through the identification of key variables using both univariate or multivariate numerical approaches. Overall, HWL periods are dominated by the transport of suspended and dissolved materials, whereas LWL periods are characterized primarily by storage, production and assimilation processes, particularly those associated with primary production. Furthermore, the lateral homogenization of physicochemical conditions and biota is most frequently reported during HWL periods. However, the diferent interpretations of the relationships between physicochemical variability and the complex hydrogeomorphic dynamics, primarily driven by variability across multiple spatiotemporal scales (for example, Thomaz et al. 2007; Castillo 2020; Lopera-Congote et al. 2020; Mayora et al. 2020; Wohl et al. 2021; Bek et al. 2025), highlight the need for approaches that more effectively explain fluctuations in the magnitude of key variables in terms of forcing and contention functions. Within this context, the analysis of the inherent variability of environmental variables through a hydrogeomorphic framework supports the hypothesis that the physicochemical variability arises from recurrent and interacting conditionsthat are associated with, but not exclusively determined by, water levels periods or or geomorphic features.

2. Methods

2.1 Study area

The PCBR is a complex net of riverine wetlands located on elevations ranging from − 1.0 a 7.0 meters above sea level (masl), with an area of 302 706.62 ha (17°57'53"–18°39'03"N, 92º06'39"–92º47'58"W) in coastal floodplain of the southern Gulf of Mexico (Romero et al. 2000). The PCBR is located in the alluvial zone of the Grijalva and Usumacinta fluvial systems, which discharge into the Southern Gulf of Mexico. Within the PCBR are approximately 110 lakes interconnected through one tributary, three distributaries and numerous natural and artificial channels (Fig. 1). Notably, one of the artificial channels, approximately 37 km long with a 3.3 m of average depth, stands out in the Usumacinta fluvial system. This channel was built between 1979 and 1981 to connect Pemex city and the Pom-Atasta fluvial lagoon system of Terminos lagoon (Brzovic 1990; INEGI 2021). The combined annual average flow of both fluvial systems (358 269 m^3 s^{-1}) is the second highest after the Mississippi-Atchafalaya fluvial system (Osburn et al. 2019). However, The Grijalva fluvial system is dammed, while the Usumacinta system remains undammed. Their intra-annual flow variation accounts for the wide fluctuation in water depth, ranging from 0.4–0.6 to 1.5-6 m in lakes between the LWL and HWL periods (Sánchez et al. 2015). The LWL corresponds to the dry season, occurring from April to May, while the HWL is caused by tropical and polar rains, peaking between September and January (Cruz-Ramírez et al. 2019a). These rainfalls increases flow and depth during HWL promoting hydraulic surface lateral connection, which in turn results in an increase in flooding areas equivalent to 2 934 km^2 and the hydraulic reconnection of temporal lakes in the PCBR (Sánchez et al. 2007; Salcedo et al. 2012). In contrast, the reduction in flow during the LWL leads to both the temporary hydraulic isolation of several lakes and the inflow of tidal currents up to 22.5 km upstream from the mouth which increases the estuarine area (Salcedo et al. 2012; Esqueda-Lara et al. 2021).

In the PCRB, the arboreal communities are dominated by *Terminalia buceras* (L.) C. Wright, *Haematoxylum campechianum* L., *Pachira aquatica* Aubl., *Rhizophora mangle* L., y *Tabebuia rosea* (Bertol.) DC., Aditiionally, among the herbaceous communities, the submersed rooted macrophytes are represented by *Vallisneria americana* Michx. and *Cabomba palaeformis* Fassett, while the floating leaf macrophytes, *Nymphaea ampla* (Salisb.) DC is the most frequent species. The free floating macrophytes dominants are *Pontederia crassipes* Mart. y *Pistia stratiotes* L. (Novelo 2006; López-Jiménez et al. 2020). At last, the emergent rooted macrophytes are mainly represented by *Dalbergia brownei*

(Jacq.) Urb., *Gynerium sagittatum* (Aubl.) P. Beauv., *Thalia geniculata* L., and *Typha domingensis* Pers. These macrophytes covered approximately el 34% of the total area of the PCRB, which decreased 5% at the beginning of this century (de la Rosa-Velázquez et al. 2017). Despite the loss of macrophyte cover area, the lateral and longitudinal surface hydraulic connectivity in the PCRB has remained largely unaltered. The currently maintenance of the lateral connectivity during the HWL in PCBR is attributed to the absence of large-scale agricultural, forestal, oil, hydraulic or urbanization megaprojects (Sánchez et al. 2015; Cruz-Ramírez et al. 2019a; Castillo et al. 2023) since its designation as protected area in 1992. The lack of such developments has been linked to the conservation of the intra-annual lateral flooding during flood pulses in fluvial systems (Junk et al. 1989; Junk 1998; Tockner et al. 2000; Poff et al. 2007).

2.2 Sampling

The 27 sampling sites were distributed throughout the alluvial zone in the Grijalva and Usumacinta river systems within the PCBR. Of these, eight were lotic (Lo) and 19 lentics (Le) (Supplementary Table S1). The lotic sites were located in main rivers, distributaries, tributaries, and one artificial channel, whereas the lentic sites were situated in lakes with permanent surface hydraulic connectivity. Two of the eight lotic sites were located along a river bank and within the artificial channel, with depths ranging from 2 to 4.2 m and from 1.3 to 5.5 m, respectively. The remaining six lotic sites had depths ranging from 1.3 to 16 m. In contrast, 19 lentic sites had depths from 0.1 to 6 m. Each site was sampled 10 nonconsecutive years between 2000 and 2017 to represent the intraannual water-level variability across an interannual period encompassing both major flood and drought conditions. The intraannual variability was assessed during two level extremes (HWL and LWL). The availability of concurrent physicochemical and biological data in the water column in both lotic and lentic environments supported the selection of five bi-annual periods (2000–2001, 2004–2005, 2007–2008, 2010–2011, 2016–2017). This sampling design yielded a total of 540 samples (27 sites x 10 replies x 2 water level periods), allowing the analysis of the fluctuations of the physicochemical parameters and phytoplankton biomass within a hydrogeomorphological framework (Figs. 1 and 2).

Eleven physicochemical variables and one biological variable were measured at each sampling site. Among these, depth (Z) in meters, transparency (SD) in meters, electrical conductivity (EC) in μS cm^{-1} and the dissolved oxygen saturation percentage (DOS) were measured *in situ* using a Hondex echosounder, Secchi disk and a multiparametric YSI, respectively (Fig. 2). Meanwhile, samples for total suspended solids (TSS), ammonium (NH_4^+), nitrates (NO_3^-), total phosphorus (TP), orthophosphate (PO_4^{3-}), biochemical oxygen demand (BOD_5) and chlorophyll *a* (Chl-*a*) in μg L^{-1} were collected from the photic zone using a van Dorn bottle. The photic zone was determined with a Secchi disk. All samples were preserved at 4°C and analysed in the laboratory according to APHA (1998) (Fig. 2). In total 5 940 data were generated from 27 sampling sites under two intra-annual water level conditions, with 10 replies and 11 variables measured (Fig. 2).

2.3 Data analysis

Three complementary approaches were used to interpret the spatiotemporal variation of physico-chemical variables within a hydrogeomorphic framework. First, 11 physicochemical and biological variables were analyzed individually to characterize the limnological conditions of the study area (see section 2.3.1). Second, key variables were identified and their spatiotemporal trends were examined using a principal component analysis (PCA) biplot (see section 2.3.1). Third, the inherent variability of the dataset was evaluated using the same eight key variables selected in the previous approach. In the first step, data for each selected variable were organized to identify the bumps associated with them (see section 2.3.2). In the second step, spatial and temporal trends in data dispersion were analysed for each key variable to assess variability across space and time (see section 2.3.3). Unlike the first two approaches, which focused on trends of variation in individual-variables level, the third approach examined the intrinsic variability of the data themselves.

2.3.1 Identification and spatio- temporal analysis of key variables

Eleven physicochemical variables and algal biomass were interpreted from a limnological perspective. This limnological characterization was based on measures of their central tendency and dispersion values. Subsequently, these variables were independently compared through geomorphic elements (Lo and Le) and intra-annual variation (HWL and LWL) using the non-parametric Wilcoxon test ($p < 0.05$). This approach was selected due to non-normal distribution of the data (Shapiro-Wilk, $p < 0.05$) and the absence of homoscedasticity (Bartlett, $p < 0.05$) as outlined by Iman (1974) and Zar (2010). The variables showing highly significant differences (Wilcoxon test, $p < 0.0001$) were selected for inclusion in a PCA to reduced data dimensionality (Gewers et al. 2021), identified key variables, and interpret the multivariate dispersion of samples across space (Lo and Le) and time (HWL and LWL) by using a biplot analysis (Fig. 2). The PCA was performed on the correlation matrix of standardized data (z-value) for the selected variables (Legendre and Legendre 2003). The selected or key variables were defined as those with absolute loadings greater than |0.4| on the principal components (PCs) with eigenvalues greater than 1, following the Kaiser-Guttman criterion, and showing significant variation (Bartlett´s test, $p < 0.05$). To identify the spatio-temporal trends, the key variables that significantly contributed to the selected PCs (Legendre and Legendre 2003, Weilhoefer et al. 2008) were interpreted by evaluating their total or partial dispersion relative to the direction of the variable vectors in the PCA biplot (Fig. 2), according to Jolliffe and Cadima (2016).

In order to identify the spatio-temporal trends of the key variables de acuerdo con Jolliffe and Cadima (2016) These variables, which significantly contributed to the selected PCs (Legendre and Legendre, 2003, Weilhoefer et al. 2008), were interpreted through the evaluation of their total or partial dispersion closest to the direction of the arrows of the key variables in the PCA biplot (Fig. 2).

2.3.2 Spatial and temporal arrangement of data by key variable

The spatial and temporal variability of the data of each key variable was analyzed through four steps: 1) generating density histograms for each key variable, 2) applying smoothing the density histograms, 3) calculating the bump area within each violin plot, and 4) quantifying the bump data ranges corresponding to each violin plots (Fig. 2).

First, the data distribution for each key variable was visualized using a density histogram, where the optimal number of bins or interval classes was determined by the Sturges´ Rule. Then, the binwidths (w_i) were calculated by dividing the range of the data by the number of bins for each key variable. Second, the violin plots by key variable were generated by smoothing the total area of the density histogram using the nonparametric Kernel Density Estimation (KDE), as proposed by Scott (2015). This normalization of the total area under the curve equals it to one (Cleveland 1979; Müller and Petersen 2016). Third, the bump area or area of maximum data point density visualized within the violin plot was calculated by summing the partial areas of the binwidths put on the mentioned area of maximum data point. Each binwidth was calculated by multiplying the height of the histogram bar by its corresponding width (Tukey 1977; Hintze and Nelson 1998). In this sense, the bump area is a relative value of the unity given by the KDE normalization of the area under the curve mentioned in the second step. Then, the key variables with bump areas greater than 0.5 were considered representative of the probability density estimation. Fourth, the bump or bumps graphically represented within each violin plot were measured by estimating the data range (Fig. 2). The number of data points within the bump was related to the total number of data points for each geomorphic element by key variable (Le = 190 or Lo = 80).

The Wilcoxon test, PCA, density histograms, smoothing curves, violin plots and estimations of the range of data in the bumps were obtained with the JMP® program version 17 (SAS Institute, Inc., Cary, NC, USA). The bump area was calculated through Microsoft Excel (2018).

2.3.3 Spatial and temporal trends of the key variables data

The spatial and temporal tendencies of the physicochemical and algal biomass were interpreted based on variations in data distribution within the bumps. This interpretation was derived from comparisons across all the spatial and temporal combinations (HWL-Lo, LWL-Lo, HWL-Lo, LWL-Le) using the bump data ranges for each of the eight key variables (Fig. 2). The area of data density and the number of data points within each bump were used as indicators of representativeness. Finally, the distribution of the key variables integrated their spatio-temporal trends identified through the arrangement of data points within the bumps, along with the limnological and biplot PCA biplot interpretations.

3. Results

3.1 Limnological characterization

The central tendency and dispersion values of the eleven physicochemical and biological variables measured in the water column during this study are summarized in the Supplementary Table S2. Most sampling sites were classified as limnetic (< 800 µS cm^{-1}), while the 20% were oligohaline. The relationship between the depth (0.1–16 m) and high TSS concentrations (> 25 mg L^{-1}) measured below the Secchi depth (≅ 1 meter) was interpreted as indicative of reduced light availability. This condition likely limited primary production and indicates increased transport of terrigenous. The average of DOS records (69 ± 36%) was linked to undersaturated conditions and degradation of organic matter in the water column. This interpretation is supported by the average BOD_5 value of 3 ± 2 mg L^{-1}. The average Chl-*a* concentration of 16.4 µg L^{-1} indicated eutrophic conditions, supported by high algal biomass production in the 79% of the samples. The trophic relationship between nutrients and production of algal biomass suggested nutrient recycling or surplus. In this context, most of NH_4^+ (98%) and NO_3^- (92%) concentrations were below 1 mg L^{-1}, which was interpreted as assimilation or recycling. In contrast, the enrichment conditions were observed for PO_4^{3-} (0.013 mg L^{-1}) and TP (0.024 mg L^{-1}) with high concentrations detected in more than 85% of the samples.

3.2. Spatial and temporal variations of the key variables

Eight of out eleven variables were identified as key because they had loadings greater than |0.4| on the first three PCs, all of which had eigenvalues greater than 1, showed significant variation (χ^2, $p < 0.0001$), and together explained 54.8% of the cumulative variance (Table 1). In PC1, SD (-0.603) was negatively associated with TSS (0.474) and DOS (0.463), while both variables were positively correlated (Fig. 3). The PC2 was characterized by a positive association between Z (0.477) and TSS (0.413), and a negative relation with EC (-0.406) (Fig. 3). The PC3 showed a positive association between NO_3^- (0.620) and Chl-*a* (0.555) and a negative association with PO_4^{3-} (-0.489) (Fig. 3).

Table 1
Loadings, eigenvalues, and variance in Principal Components Analysis of the spatial and temporal variation of physicochemical and biological variables in Pantanos de Centla Biosphere Reserve in the Grijalva and Usumacinta fluvial systems. Loadings greater than |0.4| and eigenvalues greater than 1 in each PC are in bold. SD = Secchi disk depth, TSS = total suspended solids, DOS = dissolved oxygen saturation, Z = depth, EC = electrical conductivity, NO_3^- = nitrate, Chl-*a* = chlorophyll-*a*, PO_4^{3-} = orthophosphate. n = 4 320

Variables	**PC1**	**PC2**	**PC3**
Z	0.163	**0.477**	0.132
SD	**-0.603**	0.014	-0.092
TSS	**0.474**	**0.413**	-0.072
EC	0.260	**-0.406**	0.139
DOS	**0.463**	-0.398	-0.134
NO_3^-	-0.047	0.368	**0.620**
PO_4^{3-}	0.228	0.343	**-0.489**
Chl-*a*	0.222	-0.161	**0.555**
Eigenvalue	1.776	1.501	1.11
Variance explained (%)	22.2	18.8	13.9
Variance accumulated (%)	22.2	41	**54.8**

Four tendencies were associated with whole spatial and temporal combinations (HWL-Lo, HWL-Le, LWL-Lo, LWL-Le) of the key variables. First, the HWL-Lo conditions were explained by SD, TSS, Z, NO_3^- and PO_4^{3-}. In PC1, SD showed a negative loading, while TSS was positive. In PC2, Z was positively associated due to the increment of the downriver water level. In PC3, the NO_3^- was positive, while PO_4^{3-} negative (Fig. 3). The HWL-Lo results indicated that fluvial transport of terrigenous material reached concentrations up to 218 mg L^{-1}. This was linked to increased downriver water volume under HWL periods, which reduced the light penetration (< 0.4 m). The enhanced fluvial transport likely contributed to explain the increment of NO_3^- and PO_4^{3-} greater than 0.406 and 0.059 mg L^{-1}, respectively. Second, the HWL-Le conditions were defined by SD, DOS, NO_3^-, Chl-*a* and PO_4^{3-}. In PC1, SD was negatively associated, whereas DOS was positive. In the PC3, both NO_3^- and Chl-*a* showed partial associations with the HWL-Le samples along the positive axis of these variables, while PO_4^{3-} was negative (Fig. 3). This trend indicates a water clarification and a reduction of DOS (≤ 35%), together with potential increases in NO_3^- and PO_4^{3-} concentrations, possibly due to the dilution of the phytoplankton biomass. Third, the LWL-Lo conditions were primarily defined by an inverse relationship between Z and EC in the PC2 (Fig. 3). Herein, the reduction in downriver water volume (lowest Z values) across the fluvial system was mainly linked to a possible increment of ion concentrations within the tidal influence zone. Finally, DOS, Z, EC, and Chl-*a* determined the LWL-Le conditions based on a positive association of DOS and Chl-*a* in the PC1 and PC3, respectively. Besides in PC2, Z was positive, while EC was negative associated (Fig. 3). These conditions reflect an increase in DOS under lower water levels and a possible rise in dissolved ions and algal biomass.

3.3. Spatial and temporal trends of the key variables data

Under HWL and LWL periods, the lotic Z data exhibited a bimodal distribution reflecting the contrasting arrangement of their data points linked to the river´s maximum depths and two shallow sites (an artificial channel and a riverbank). In contrast as expected, the lentic Z data displayed a unimodal distribution at both temporal conditions (Fig. 4). The Z bump ranges in HWL and LWL river sites were noticeably deeper (Table 2) than those observed in the bumps corresponding to the two shallow sites (artificial channel and riverbank), with minimal overlap between the respective Z bumps (Fig. 4). Instead, the Z bump range of the two shallow lotic sites overlapped with the other two combinations recorded under LWL conditions. Notably, the maximum data points in both the bump and violin plot under LWL-Le were shallower to the other three spatio-temporal conditions (Table 2).

3.3.1 Fluvial conditions

The maximum TSS values were measured in HWL-Lo conditions, where the data points exceeding 122 mg L^{-1} were registered exclusively in this spatio-temporal condition, though these data represented less than 16% of this violin plot (Fig. 4). Moreover, in the upper range in the HWL-Lo TSS bump (39 to 58 mg L^{-1}), counting 28% of bump data, resulted higher from the other three spatio-temporal conditions. Instead, the TSS values below 39 mg L^{-1} showed a substantial overlap among the four spatio-temporal bumps conditions (Fig. 4; Table 2).

Overall, the violin plot shapes for PO_4^{3-} and NO_3^- were similar across all four spatio-temporal conditions (Fig. 4), with a remarkable overlap of data points below 0.049 mg L^{-1} and 0.593 mg L^{-1}, respectively (Table 2). Additionally, the PO_4^{3-} bump accounted for 76% of the total violin plot area, while the NO_3^- bump area comprised 85% (Table 2). The PO_4^{3-} concentrations ranging from 0.048 to 0.096 mg L^{-1} represented almost half (43%) of the total HWL-Lo bump area and they did not overlap with data bumps from other three spatio-temporal conditions (Fig. 4). The remaining 24% of PO_4^{3-} data points were located above the upper limit of the HWL-Lo bump (> 0.096 mg L^{-1}) (Table 2), coinciding with the highest TSS values indicative of fluvial transport. Similarly, 16% of NO_3^- data points, ranging from 0.593 to 0.764 mg L^{-1} lay exclusively within this river bump (Fig. 4; Table 2).

3.3.2 Lateral homogenization conditions

Although SD depth data points within the bumps largely overlapped below 0.9 m across the four spatio-temporal conditions, the shapes of the violin plots differed substantially between HWL and LWL periods (Fig. 4). Specifically, the four bumps showed notably overlap within the 0.1–0.5 m depth range representing 62% of the data points within the four bumps highlighted the prevalence of reduced light availability in all spatio-temporal conditions, affecting both lotic and lakes ecosystems. The data points above 0.9 m, recorded only during HWL showed clarification conditions, but accounted for only 37% of the total data points (Table 2).

In contrast to SD trends, both the violin plot shapes and bump distributions of the DOS data points were lower under HWL periods compared to LWL conditions (Fig. 4). The overlap between the HWL bumps ranged from 3 to 78% of DOS, while in LWL conditions was from 70 to 99% (Table 2). Under HWL periods, the bumps accounted for 85% and 90% of the total DOS data in lotic and lake ecosystems, respectively, and were characterized by undersaturated DOS conditions. These bumps were predominantly composed of hypoxic values (≤ 49% DOS), which represented at least 55% of their data points (Table 2). Conversely, during LWL conditions, all of the data points in both bumps surpassed 70% of DOS, indicating undersaturated conditions without any record of hypoxic values (Table 2). Notably, only under LWL-Le conditions, the 12% of the upper violin plot data points exceeded 100% of DOS, indicating hypersaturation of dissolved oxygen.

Similar to DOS, both the violin plot shapes and bump distributions of the EC data points were lower under HWL periods than LWL conditions (Fig. 4). In HWL periods, the upper bump data points remained below 399 µS cm^{-1}, with maximum values reaching 1 317 µS cm^{-1} (Table 2), suggesting ion dilution under these conditions associated with the river level increment (Fig. 4). In contrast, during LWL, 18% of the bump data points exceeded 399 µS cm^{-1}, reaching up to 793 in lentic and 999 µS cm^{-1} in lotic ecosystems. These elevated values may be linked to the reduced influence of tidal currents during periods of diminished river flow (Table 2). However, the oligohaline conditions (> 793 µS cm^{-1}) only represented less than 32% of the data points, which were placed outside the bumps. Furthermore, the limnetic conditions prevailed across all four hydrogeomorphic conditions (Table 2).

3.3.3 Lentic low water level conditions

A total of 83% of the Chl-*a* bump data points overlapped across the four spatial-temporal conditions, with the upper data points remaining below 19.3 µg L^{-1}. The few data points exceeding 19.3 µg L^{-1} within the bumps occurred specifically under LWL-Le conditions, where 27% of the bump data points ranged from 19.3 to 24.6 µg L^{-1} (Table 2). This eutrophic condition in LWL-Le coincided with hypersaturation of dissolved oxygen and the shallowest Z data points recorded in lakes, as previously described (Fig. 4). Additionally, occasional data points above the bumps indicated hypereutrophic conditions (> 25 µg L^{-1}) across the four violin plots (Fig. 4).

4. Discussion

Forcing functions, especially water kinetic energy, are key environmental regulators of fluvial systems (Ward 1989; Wantzen et al. 2008; Tian et al. 2024; Feng et al. 2025; Zhang 2025). Within the PCBR, located within the alluvial zone of the Usumacinta and Grijalva fluvial systems, the interpretation of the spatiotemporal variability of Z data points variability reorganized the distribution trends of the key variables into three energy conditions. The first represented to high-energy fluvial conditions during the HWL period. The second corresponded lateral homogenization conditions (LHC) linked to the temporal variation under LWL in rivers and HWL in lakes. The third comprised low energy conditions confined to lakes during LWL periods in lakes (LWL-LeC). Elevated water levels were stongly associated with the highest TSS values and nutrient enrichment, indicating intensified hydrological connectivity and material transport under fluvial dominated HWL periods. These findings partially agrees with Junk (2002), Dodds and Whiles (2004), Junk et al. (2015), Keogh et al. (2019), Evans et al. (2021) and Primost et al. (2022). Conversely, lateral homogenization was detected under both water level periods (LWL and HWL), as was reflected in the convergence of the data points distribution for the light penetration (attenuation), DOS and EC values in both lakes and rivers. This homogenization may be attributable to permanent surface hydraulic interconnectivity, a process previously reported during HWL periods by Thomaz et al. (2007), and during LWL periods by Bek et al. (2025). Finally, the eutrophic and DOS supersaturation conditions were measured exclusively in the lakes during LWL periods. These observations are consistent with those published by Junk et al. (1989, 2015); Covino (2017); Stevens et al. (2025). Such eutrophic and DOS supersaturation conditions have been associated with declining water levels and prolonged water residence times, which enhance nutrient retention, primary productivity, and biogeochemical processing within lentic environments (Covino 2017; Chaparro et al. 2023).

Table 2

The spatial (Lo and Le) and temporal (LWL and HWL) variability of the data of the key variables in Pantanos de Centla Biosphere Reserve in the Grijalva and Usumacinta fluvial systems. Lotic (Lo), lentic (Le), Low water level (LWL), High water level (HWL). Z = depth, TSS = total suspended solids, SD = Secchi disk depth, DOS = dissolved oxygen saturation, NO_3^- = nitrate, PO_4^{3-} = orthophosphate, EC = electrical conductivity, and Chl-*a* = chlorophyll-*a*. Number of bump data points (Bn), number of data points by geomorphic element (Gn), bump area (Ba), bump range (range B), range of the key variable (T range), rivers (r), and artificial channel and riverbank (ac-b), and * = bimodal distribution

Variable	Space-Time	Bn	Gn	Ba	range B	T range
Z (m)	HWL-Lo (r)*	33	39	0.41	11.5–16.0	1.7–16.0
	HWL-Lo (ac-b)*	31	41	0.39	1.7–5.5	1.7–16.0
	HWL-Le	132	190	0.69	1.0-2.9	0.4-6.0
	LWL- Lo (r)*	36	37	0.45	7.0–12.0	1.3–15.0
	LWL-Lo (ac-b)*	31	43	0.39	1.3–4.3	1.3–15.0
	LWL-Le	176	190	0.93	0.1–1.9	0.1–2.7
TSS (mg L^{-1})	HWL-Lo	53	80	0.66	1–58	1-218
	HWL-Le	150	190	0.79	0–19	0–71
	LWL-Lo	63	80	0.79	2–28	2-122
	LWL-Le	164	190	0.86	1–39	1–77
SD (m)	HWL-Lo	64	80	0.80	0.1–0.7	0.1–3.1
	HWL-Le	103	190	0.54	0.2–0.9	0.2–3.5
	LWL-Lo	72	80	0.90	0.4–0.9	0.1–1.3
	LWL-Le	172	190	0.95	0.2–0.8	0.1-1.0
DOS (%)	HWL-Lo	68	80	0.85	1–77	1-108
	HWL-Le	170	190	0.90	3–78	3-122
	LWL-Lo	61	80	0.76	73–99	17–148
	LWL-Le	135	190	0.71	70–109	35–179
NO_3^- (mg L^{-1})	HWL-Lo	68	80	0.85	0.004–0.764	0.004–2.759
	HWL-Le	141	190	0.74	0.004–0.593	0.004–2.706
	LWL-Lo	64	80	0.80	0.003–0.580	0.003–2.520
	LWL-Le	159	190	0.84	0.007–0.583	0.007–3.652
PO_4^{3-} (mg L^{-1})	HWL-Lo	61	80	0.76	0.001–0.096	0.001–0.439
	HWL-Le	137	190	0.72	0.001–0.048	0.001–0.442
	LWL-Lo	59	80	0.74	0.001–0.048	0.001–0.274
	LWL-Le	145	190	0.76	0.001–0.049	0.001–0.373

Variable	Space-Time	Bn	Gn	Ba	range B	T range
EC (µS cm^{-1})	HWL-Lo	54	80	0.68	209–397	209–857
	HWL-Le	133	190	0.70	212–399	198–1317
	LWL-Lo	55	80	0.69	257–999	257–4150
	LWL-Le	138	190	0.73	216–793	216–3798
Chl-*a* (µg L^{-1})	HWL-Lo	58	80	0.73	10.7–18.3	5.3–53.4
	HWL-Le	143	190	0.75	10.7–19.3	4.0-80.1
	LWL-Lo	55	80	0.69	10.2–18.3	5.0–32.0
	LWL-Le	135	190	0.71	10.7–24.6	5.3–42.7

a) **Fluvial condition**

During HWL periods, water levels exceeding 11.5 m in the Usumacinta river (as represented in the upper bump) were associated with intense fluvial transport of sediments and nutrient enrichment driven by strong hydraulic lateral hydrological connectivity and high kinetic energy. This dynamic promoted the exchange and biogeochemical processing of inorganic and organic materials between channels and lakes is consistent with numerous results previously published (for example, Ward 1989; Dunne and Aalto 2013; Keogh et al. 2019; Wohl et al. 2021; Arfania et al. 2025). In particular, the transport of TSS, nitrates and orthophosphates reached highest its highest levels before September when the water level frequently gets over the bankfull stage. In the Usumacinta fluvial system bankfull conditions happens when the main river reaches 15 masl (Medrano-Pérez et al. 2022).

In the PCBR, TSS values above 80 mg L^{-1} may be related to the deforestation rates of 42–45%, previously reported upstream in the Usumacinta and Grijalva fluvial systems by Sandoval-Rivera et al. (2022). Additionally, 45% of the TSS bump data fell within the 30 to 60 mg L^{-1} range, which corresponds to moderate sediment transport reported for rivers in Asia, the United States, and South America (Adjovu et al. 2023). These TSS values have been linked to hydric erosion, increased fluvial transport of nutrients, and modified their attenuation within the wetland (Dodds and Whiles 2004; Primost et al. 2022). Regarding the frequently reported link between aquatic nutrient enrichment and agricultural land use upstream or in surroundings areas (Wetzel 2001; Primost et al. 2022; Savenko and Savenko 2022), the nutrient enrichment detected during the fluvial conditions in the PCBR and other fluvial systems (Mathers et al. 2024) may also reflected to that almost half of the reported land use changes upstream has been converted to agricultural activities (Sandoval-Rivera et al. 2022). For example, the increases in PO_4^{3-} and NO_3^- concentrations transported fluvially into the PCBR are partially consistent with values reported for the Comoé river (0.04 a 0.1 mg L^{-1}) and Arikaree River (0.5 a 0.9 mg L^{-1}) by Soro et al. (2020) and Kermorvant et al. (2023), respectively. Similarly, residual discharges combined with agricultural fertilization has been cited as drivers of NO_3^- enrichment in the lower Yellow River (Zhang 2025).

Unlike the fluvial conditions registered in the PCBR, the nutrient assimilation was enhanced under both LHC and LWL-LeC conditions. Overall, the NO_3^- (< 0.5 mg L^{-1}) and PO_4^{3-} (< 0.068 mg L^{-1}) values measured during both conditions were consistent with assimilation conditions reported for other wetlands (Rendón et al. 2016; Lane et al. 2018; Cruz-Ramírez et al. 2019a; Vero et al. 2019; Preiner et al. 2020; Day et al. 2021; Walalite et al. 2023). In the PCBR, these reduced NO_3^- and PO_4^{3-} concentrations likely refelect lower flow kinetic energy during the LHC under LWL conditions, coupled with sustained nutrient uptake by aquatic macrophytes and phytoplankton. This interpretation is supported by the perennial presence of aquatic macrophytes combined with the increase in Chl-*a* concentrations during LWL conditions (Novelo 2006; Sánchez et al. 2012; de la Rosa-Velázquez et al. 2017; Sánchez et al. 2024) likely contributed

to the observed nutrient reduction, as has also been reported for other riverine wetlands (Wetzel 2001; Roach et al. 2014; Cruz-Ramírez et al. 2019a; Primost et al. 2022).

Under fluvial conditions, the presence of man-made channels within the longitudinal alluvial zone may locally restrains the lateral connectivity, particularly near in the bottom, by diverting flow, reducing water velocity, and enhancing the sediment deposition and nutrients concentrations (Mel et al. 2020; Serra-Llobet et al. 2022; Argillier et al. 2025; Qiao et al. 2025). For example in the Narváez channel, the average PO_4^{3-} concentrations and DOS differed from those measured under fluvial conditions, since the PO_4^{3-} concentrations were 56% higher, whereas DOS values were 20% lower than those recorded during fluvial conditions. The coexixtence of hypoxic conditions, accumulation of PO_4^{3-} and associated cyanobacterial blooms in the artificial channels has been hypothetized as a contributing factor to the mass mortality of manatees recorded in the PCBR (O'Shea et al. 2018; PROFEPA 2018). Furthermore, the hypoxic conditions measured in the Narváez channel are consistent with the DOS values reported for artificial channeles along the West coast of Southwestern Australia (Cronin-O'Reilly et al. 2025), suggesting that reduced water circulation and prolonged residence times may promote similar ecological responses across geographically distinct systems.

b) Lateral homogenization condition (LHC)

In contrast to the fluvial conditions, the spatial homogenization of EC, SD and DOS values across the two geomorphic elements resulted independent of water level fluctuations (HWL or LWL) in the PCBR. Overall, the LHC have been reported more frequently during HLW periods than under LWL periods in other fluvial systems (Thomaz et al. 2007; de Wilde et al. 2015; Castillo 2020; Shen and Liu 2021), as flood pulses enhance lateral hydrological connectivity by overflowing lakes and floodplains during the HWL periods (Thomaz et al. 2007; Mayr et al. 2020; Wohl et al. 2021; Brinkerhoff et al. 2026). By contrast, under LWL periods, LHC has been linked to lakes with permanent surface connectivity with rivers through connecting channels (Arfania et al. 2025).

Under HWL conditions, the EC values were similar in lakes (212 to 399 µS cm^{-1}) and rivers (209 to 397 µS cm^{-1}). The substantial increase in depth, reaching up to 16 m in the Usumacinta river, promoted the lateral homogenization through both dilution of the river water and overbank flooding. This homogenization is consistent with the results reported from the Vasse–Wonnerup estuary (Australia), where reductions in salinity were associated with increases in water level and intense rainfall events (Cronin-O'Reilly et al. 2025). Conversely, EC increased to 999 µS cm^{-1} when the water level dropped to 7 m in the Usumacinta river due to seasonal rise in evaporation and stronger tidal influence during the LWL in the PCBR. The lateral homogenization of SD and DOS is a consequence to enhanced transport and redistribution of suspended solids across the floodplain (lateral dimension) during HWL conditions (Gugliotta et al. 2020; Adjovu et al. 2023). These homogenization tends of are linked to the river overflow and the widespread dispersal of sediments driven by flood pulses (Thomaz et al. 2007; Adjovu et al. 2023). In the PCBR, these processes coincided with low light penetration (SD < 0.9 m) and DOS undersaturated (< 78%) conditions. Furthermore, the LHC registers of SD under HWL periods have been measured in interconnected lotic and lentic ecosystems in the Mississippi Delta and one Amazonic wetland (Thomaz et al. 2007; Day et al. 2021), as well as in the Kopački Rit floodplain in Croatia (Bek et al. 2025), respectively.

During LWL periods, the LHC promoted the redistribution of suspended and dissolved materials, thereby reducing spatial gradients throughout the floodplain (de Wilde et al. 2015; Shen and Liu 2021). The restriction of light penetration likely contributed to the generally DOS undersaturated condition (< 99%) measured across the PCBR, which was previously reported by Salcedo et al. (2012) and Castillo (2020). Furthermore, DOS undersaturated values during LWL periods may have been reinforced by elevate water temperature (de Wilde et al. 2015; Jeppesen et al. 2015; Zhang 2025) and dropped water depth (Lopera-Congote et al. 2020). These conditions were consistent with those recorded during the LWL period in the study area.

c) Lentic low water level conditions (LWL-LeC)

Forcing and constraining functions (Wantzen et al. 2008; Guseva et al. 2021; Zhang and Chen 2023), generated by the altitudinal gradients across the lateral dimensión of fluvial systems, have proven useful for understanding both fluctuations in water and materials input, and their residence times within lakes (Li et al. 2019; Mayora et al. 2020; Gracia et al. 2023; Zhang 2025). In the PCBR, the altitudinal differences between the main river channel (1.23 masl) and the adjacent floodplain (–1 masl) reported by SEMARNAT (2000) and Medrano-Pérez et al. (2022), may help explain the occurrence of LWL-LeC. In particular, these conditions were characterized by a predominance trend of high eutrophic (> 19.3 µg L^{-1}) and hypereutrophic Chl-*a* concentrations, since the hypereutrophic data points represented 27% of in the violin plot of LWL-Le (Fig. 4). The Chl-*a* hypereutrophic conditions were linked to the DOS supersaturation (109%) on the shallowest Z values (< 0.9 m) in lakes with extended water residence times. This pattern in consistent with observations from lakes in the Donau-Auen National Park, Vienna, Austria, and from lakes hydrologically connected to the Danube river (Covino 2017; Chaparro et al. 2023).

Overall, HWL-Le conditions function as sinks for both of organic and inorganic matter, reducing DOS and promoting the development of eutrophic conditions in lakes (Tockner et al. 2000; Shuhaimi-Othman et al. 2007; Cruz-Ramírez et al. 2019a; Carhart et al. 2021). These eutrophic conditions in lakes may be temporary or persist for extended periods, depending on hydrological connectivity and water residence time. In lakes permanently connected or subject to temporal LHC periods, the high phytoplankton biomass is recycled within the trophic web and exported as Chl-*a* or faunal biomass to interconnected ecosystems when the water levels increase (Carlson 2007; Thomaz et al. 2007; Cruz-Ramírez et al. 2019a; Sánchez et al. 2019; Liu et al. 2024; Jeethu and Kaladevi 2025). In contrast, hypereutrophic conditions may persist throughout the year or across multiple years in lakes with severely restricted hydraulic connectivity o in permanently isolated (Cruz-Ramírez et al. 2019b; Zou et al. 2020; Salcedo et al. 2022). Moreover, these persistent hypereutrophic conditions can be further intensified in isolated lakes by external inputs of organic matter derived from urban and agricultural activities (Cruz-Ramírez et al. 2019b; Zou et al. 2020; Salcedo et al. 2022).

5. Conclusions

The physicochemical and biological variability in the water column was examined using three complementary approaches: i) a limnological characterization based on central tendency and dispersion values for 11 variables, ii) an assessment of total and partial dispersion through a PCA biplot derived from eight key variables across two water level periods and two geomorphic elements (rivers and lakes), and iii) an evaluation of the inherent variability of the inherent variability of these eight key variables within the same spatio-temporal framework. The first two approaches focused on variability at the level of individualcvariables. Both only provided a partial explanation of physicochemical and biological variability in the water column. In particular, the second approach identified four conditions (HWL-Lo, HWL-Le, LWL-Lo, LWL-Le) corresponding to the spatial and temporal combinations defined by the sampling design. However, neither approach provided enough support for the proposed hypothesis. Instead, the third approach focused on the intrinsic variability of the data rather than on individual variables level, enabling a direct evaluation of the proposed hypothesis. This analysis revealed that recurrent and interacting patterns of variability in key variables were organized into three hydrogeomorphic conditions: fluvial, lateral homogenization and lentic low water level. Within this framework, the analysis of data variability proved to be an useful tool for understanding water column dynamics and identifying the principal hydrogeomorphic conditions regulating the ecological functioning of tropical riverine wetlands.

References

1. Adjovu GE, Stephen H, James D, Ahmad S (2023) Measurement of Total Dissolved Solids and Total Suspended Solids in Water Systems: A Review of the Issues, Conventional, and Remote Sensing Techniques. Remote Sens

15:3534. https://doi.org/10.3390/rs15143534

2. Amoros C, Bornette G (2002) Connectivity and biocomplexity in waterbodies of riverine floodplains. Freshw Biol 47:761–776. https://doi.org/10.1046/j.1365-2427.2002.00905.x
3. APHA (1998) Standard methods for the examination of water and wastewater, 20th edn. APHA, Washington DC
4. Arfania H, Bashir S, Aktar A, Kayler ZE (2025) Phosphorus legacy and equilibrium dynamics in up and downstream sediments of Lake Urmia. Int J Environ Sci Technol 22:13377–13392. https://doi.org/10.1007/s13762-025-06443-z
5. Argillier C, Bakken TH, Carriere A, Ciampittiello M, Hussner A, Koehler R, Kolada A et al (2025) A guide for assessing the hydromorphological quality of natural and artificial lakes. Publications Office of the European Union. https://data.europa.eu/doi/ 10.2760/2602647
6. Arisanty D, Saputra AN (2017) Remote Sensing Studies of Suspended Sediment Concentration Variation in Barito Delta. IOP Conf Ser Earth Environ Sci 98:012058. https://doi.org/10.1088/1755-1315/98/1/012058
7. Bek N, Selak L, Špoljarić Maronić D, Stević F, Pjevac P, Galir A, Orlić S et al (2025) Hydrological variability and connectivity shape floodplain microbial community dynamics. Limnol Oceanogr 70:3867–3882. https://doi.org/10.1002/lno.70263
8. Brinkerhoff CB, Raymond PA, Gleason CJ (2026) River-floodplain exchange influences basin-scale mixing during large fluvial flood events. Geophys Res Lett 53. https://doi.org/10.1029/2026GL122190. :e2026GL122190
9. Brzovic PFJ (1990) Casos de estudio de impacto ambiental: obras para el gasoducto Atasta-Ciudad PEMEX en la laguna Pom, México. Comisión Económica para América Latina y el Caribe, LC/R. 859. https://repositorio.cepal.org/entities/publication/b6b61fad-01f7-4da6-8b6c-9686ab161ce7
10. Carhart AM, Kalas JE, Rogala JT, Rohweder JJ, Drake DC, Houser JN (2021) Understanding Constraints on Submersed Vegetation Distribution in a Large, Floodplain River: the Role of Water Level Fluctuations, Water Clarity and River Geomorphology. Wetlands 41:57. https://doi.org/10.1007/s13157-021-01454-1
11. Carlson RE (2007) Estimating Trophic State. Lake Line 27:25–28
12. Carlson RE, Havens KE (2005) Simple Graphical Methods for the Interpretation of Relationships Between Trophic State Variables. Lake Reserv Manag 21:107–118. https://doi.org/10.1080/07438140509354418
13. Castillo MM (2020) Suspended sediment, nutrients, and chlorophyll in tropical floodplain lakes with different patterns of hydrological connectivity. Limnologica 82:125767. https://doi.org/10.1016/j.limno.2020.125767
14. Castillo MM, Carrillo L, Jarquín-Sánchez A, Alcérreca-Huerta JC, Álvarez-Merino M, Lázaro-Vázquez A (2023) Transport of nutrients into the southern Gulf of Mexico by the Grijalva–Usumacinta rivers. Hydrol Process 37:e14838. https://doi.org/10.1002/hyp.14838
15. Chaparro G, O'Farrell I, Hein T (2023) Hydrological conditions determine shifts of plankton metacommunity structure in riverine floodplains without affecting patterns of species richness along connectivity gradients. Aquat Sci 85:4. https://doi.org/10.1007/s00027-023-00937-z
16. Cleveland WS (1979) Robust locally weighted regression and smoothing scatterplots. J Am Stat Assoc 74:829–836. https://doi.org/10.2307/2286407
17. Covino T (2017) Hydrologic connectivity as a framework for understanding biogeochemical flux through watersheds and along fluvial networks. Geomorphology 277:133–144. https://doi.org/10.1016/j.geomorph.2016.09.030
18. Cronin-O'Reilly S, Cottingham A, Kalnejais LH, Lynch K, Tweedley JR (2025) Tidal Exclusion Barriers Fragment an Invertebrate Community into Taxonomically and Functionally Distinct Estuarine and Wetland Assemblages. J Mar Sci Eng 13:635. https://doi.org/10.3390/jmse13040635
19. Cruz-Ramírez AK, Salcedo MA, Sánchez AJ, Barba-Macías E, Mendoza-Palacios JD (2019a) Relationship among physicochemical conditions, chlorophyll-a concentration, and water level in a tropical river–floodplain system. Int J

Environ Sci Technol 16:3869–3876. https://doi.org/10.1007/s13762-018-2127-7

20. Cruz-Ramírez AK, Salcedo MA, Sánchez AJ, Mendoza-Palacios JD, Barba-Macías E, Álvarez-Pliego N, Florido R (2019b) Intra-annual variation of chlorophyll-a and nutrients in a hydraulically perturbed river-floodplain system in the Grijalva River basin. Hidrobiológica 29:163–170
21. Day JW, Conner WH, DeLaune RD, Hopkinson CS, Hunter RG, Shaffer GP, Kandalepas D et al (2021) A Review of 50 Years of Study of Hydrology, Wetland Dynamics. Aquatic Metabolism, Water Quality and Trophic Status, and Nutrient Biogeochemistry in the Barataria Basin, Mississippi Delta—System Functioning, Human Impacts and Restoration Approaches. Water 13:642. https://doi.org/10.3390/w13050642
22. de la Rosa-Velázquez MI, Espinoza-Tenorio A, Díaz-Perera MÁ, Ortega-Argueta A, Ramos-Reyes R, Espejel I (2017) Development stressors are stronger than protected area management: A case of the Pantanos de Centla Biosphere Reserve, Mexico. Land Use Policy 67:340–351. https://doi.org/10.1016/j.landusepol.2017.06.009
23. de Wilde MD, Puijalon S, Vallier F, Bornette G (2015) Physico-chemical consequences of water-level decreases in wetlands. Wetlands 35:683–694. https://doi.org/10.1007/s13157-015-0658-y
24. Diaz RJ, Breitburg DL (2009) The Hypoxic Environment. Chapter 1. Fish Physiol 27:1–23. https://doi.org/10.1016/S1546-5098(08)00001-0
25. Dodds WK, Whiles MR (2004) Quality and quantity of suspended particles in rivers: continent-scale patterns in the United States. Environ Manag 33:355–367. https://doi.org/10.1007/s00267-003-0089-z
26. Dunne T, Aalto RE (2013) Large river floodplains. In: Wohl E (ed) Treatise on geomorphology, fluvial geomorphology, vol 9. Academic, San Diego, pp 645–678
27. Esqueda-Lara K, Sánchez AJ, Salcedo MA, Rincones-Reyes KM, Popoca-Cruz PE (2021) Morfoespecies de fitoplancton de la laguna el cometa en la reserva de la biosfera pantanos de Centla. Ecosist Recur Agropecu Num Esp I e2707. https://doi.org/10.19136/era.a8nI.2707
28. Evans JL, Murdock JN, Taylor JM, Lizotte RE Jr (2021) Sediment nutrient flux rates in a shallow, turbid lake are more dependent on water quality than lake depth. Water 13:1344. https://doi.org/10.3390/w13101344
29. Evenson GR, Golden HE, Lane CR, McLaughlin DL, D'Amico E (2018) Depressional wetlands affect watershed hydrological, biogeochemical, and ecological functions. Ecol Appl 28:953–966. https://doi.org/10.1002/eap.1701
30. Feng D, Tan Z, Pinel S, Xu D, Fernandes Amaral JH, Fassoni-Andrade AC, Bonnet MP et al (2025) Drivers and impacts of sediment deposition in Amazonian floodplains. Nat Commun 16:3148. https://doi.org/10.1038/s41467-025-57495-1
31. Gewers FL, Ferreira GR, de Arruda HF, Silva FN, Comin CH, Amancio DR, Costa L (2021) da F Principal Component Analysis: A Natural Approach to Data Exploration. ACM Comput Surv 54:1–34. https://doi.org/10.1145/3447755
32. Gracia FJ, Castañeda C, Simarro G, Calvete D, Latorre B (2023) Water level control on coastal landform distribution and associated processes in a highly fluctuating shallow lake (Gallocanta Lake, NE Spain). Earth Surf Process Land 49:770–786. https://doi.org/10.1002/esp.5735
33. Gugliotta M, Saito Y, Tac TKO, Nguyen VL, Uehara K, Tamura T, Nakashima R et al (2020) Sediment distribution along the fluvial to marine transition zone of the Dong Nai River System, southern Vietnam. Mar Geol 429:106314. https://doi.org/10.1016/j.margeo.2020.106314
34. Guseva S, Casper P, Sachs T, Spank U, Lorke A (2021) Energy Flux Paths in Lakes and Reservoirs. Water 13:3270. https://doi.org/10.3390/w13223270
35. Hintze JL, Nelson RD (1998) Violin Plots: A Box Plot-Density Trace Synergism. Am Stat 52:181–184. https://doi.org/10.1080/00031305.1998.10480559
36. Iman RL (1974) Use of a t-statistic as an approximation to the exact distribution of Wilcoxon signed ranks test statistic. Commun Stat Simul Comput 3:795–806. https://doi.org/10.1080/03610927408827178

37. INEGI (2021) SIATL v4: Simulador de flujos de agua de cuencas hidrográficas. Instituto Nacional de Estadística y Geografía. https://antares.inegi.org.mx/analisis/red_hidro/siatl/. Accessed 16 May 2023
38. Jeethu JC, Kaladevi V (2025) Wetlands and Climate Change Resilience. J Clim Change 11:274–286. https://doi.org/10.70917/jcc-2025-019
39. Jeppesen E, Brucet S, Naselli-Flores L, Papastergiadou E, Stefanidis K, Nõges T, Nõges P et al (2015) Ecological impacts of global warming and water abstraction on lakes and reservoirs due to changes in water level and related changes in salinity. Hydrobiologia 750:201–227. https://doi.org/10.1007/s10750-014-2169-x
40. Jolliffe IT, Cadima J (2016) Principal component analysis: a review and recent developments. Philos Trans R Soc A 374:20150202. https://doi.org/10.1098/rsta.2015.0202
41. Junk WJ (1998) The flood pulse concept of large rivers: Learning from the tropics. Arch Hydrobiol Suppl 115:261–280. https://doi.org/10.1080/03680770.1998.11901733
42. Junk WJ (2002) Long-term environmental trends and the future of tropical wetlands. Environ Conserv 29:414–435. https://doi.org/10.1017/S0376892902000310
43. Junk WJ, Bayley PB, Sparks RE (1989) The flood pulse concept in river-floodplain systems. Can Spec Publ Fish Aquat Sci 106:110–127
44. Junk WJ, Wittmann F, Schöngart J, Piedade MTF (2015) A classification of the major habitats of Amazonian black-water river floodplains and a comparison with their white-water counterparts. Wetlands Ecol Manag 23:677–693. https://doi.org/10.1007/s11273-015-9412-8
45. Keogh ME, Kolker AS, Snedden GA, Renfro AA (2019) Hydrodynamic controls on sediment retention in an emerging diversion-fed delta. Geomorphology 332:100–111. https://doi.org/10.1016/j.geomorph.2019.02.008
46. Kermorvant C, Liquet B, Litt G, Mengersen K, Peterson EE, Hyndman RJ, Jones JB et al (2023) Understanding links between water-quality variables and nitrate concentration in freshwater streams using high frequency sensor data. PLoS ONE 18:e0287640. https://doi.org/10.1371/journal.pone.0287640
47. Lane CR, Scott GL, Autrey BC, LeDuc SD, Alexander LC (2018) Hydrological, Physical, and Chemical Functions and Connectivity of Non-Floodplain Wetlands to Downstream Waters: A Review. J Am Water Resour Assoc 54:1–26. https://doi.org/10.1111/1752-1688.12633
48. Legendre P, Legendre L (2003) Numerical ecology, 2nd edn. Elsevier Science B. V
49. Li Y, Zhang Q, Cai Y, Tan Z, Wu H, Liu X, Yao J (2019) Hydrodynamic investigation of surface hydrological connectivity and its effects on the water quality of seasonal lakes: Insights from a complex floodplain setting (Poyang Lake, China). Sci Total Environ 660:245–259. https://doi.org/10.1016/j.scitotenv.2019.01.015
50. Liu L, Huang Q, Wu Y, Arhonditsis G, Wang T, Cao Y, Fang C (2024) An ensemble modeling framework to elucidate the regulatory factors of chlorophyll-a concentrations in the Nanji wetland waters of Poyang Lake. Ecol Inf 82:102729. https://doi.org/10.1016/j.ecoinf.2024.102729
51. Liu X, Wang H (2018) Effects of loss of lateral hydrological connectivity on fish functional diversity. Conserv Biol 32:1336–1345. https://doi.org/10.1111/cobi.13142
52. Lopera-Congote L, Salgado J, Vélez MI, Link A, González-Arango C (2020) River connectivity and climate behind the long-term evolution of tropical American floodplain lakes. Ecol Evol 10:1–19. https://doi.org/10.1002/ece3.7674
53. López-Jiménez LN, López-Jiménez DA, Castillo-Acosta O, Gallardo-Cruz JA, Fernández-Montes de Oca AI (2020) Plantas vasculares de la Reserva de la Biosfera Pantanos de Centla, México. Bot Sci 98:159–204. https://doi.org/10.17129/botsci.2279
54. Marton JM, Creed IF, Lewis DB, Lane CR, Basu NB, Cohen MJ, Craft CB (2015) Geographically isolated Wetlands are important biogeochemical reactors on the landscape. Bioscience 65:408–418. https://doi.org/10.1093/biosci/biv009

55. Mathers KL, Robinson CT, Hill M, Kowarik C, Heino J, Deacon C, Weber C (2024) How effective are ecological metrics in supporting conservation and management in degraded streams? Biodivers Conserv 33:3981–4002. https://doi.org/10.1007/s10531-024-02933-7
56. Mayora G, Scarabotti P, Schneider B, Alvarenga P, Marchese M (2020) Multiscale environmental heterogeneity in a large river-floodplain systems. J South Am Earth Sci 102:102546. https://doi.org/10.1016/j.jsames.2020.102546
57. Mayr MJ, Besemer K, Sieczko A, Demeter K, Peduzzi P (2020) Bacterial community composition and function along spatiotemporal connectivity gradients in the Danube floodplain (Vienna, Austria). Aquat Sci 82:28. https://doi.org/10.1007/s00027-020-0700-x
58. McInerney PJ, Holt G, Lester RE, Thompson RM, Robson B, Ryder DS, Bond NR et al (2020) Basal resource quality and energy sources in three habitats of a lowland river ecosystem. Limnol Oceanogr 65(11):2757–2771. https://doi.org/10.1002/lno.11548
59. Medrano-Pérez OR, Payano Almánzar R, López-Jiménez LN (2022) Caracterización geomorfológica e hidroclimatológica de la Reserva de la Biósfera Pantanos de Centla. México Acta Univ 31:1–19. https://doi.org/10.15174/au.2021.2846
60. Mel RA, Viero DP, Carniello L, D'Alpaos L (2020) Multipurpose Use of Artificial Channel Networks for Flood Risk Reduction: The Case of the Waterway Padova–Venice (Italy). Water 12:1609. https://doi.org/10.3390/w12061609
61. Microsoft Corporation (2018) Microsoft Excel. Version 16.0. https://office.microsoft.com/excel
62. Müller HG, Petersen A (2016) Density Estimation Including Examples. Wiley StatsRef Stat Ref Online 1–12. https://doi.org/10.1002/9781118445112.stat02
63. Novelo RA (2006) Plantas acuáticas de la Reserva de la Biosfera Pantanos de Centla. Espacios Naturales y Desarrollo Sustentable AC, México DF
64. Obolewski K, Glińska-Lewczuk K, Bąkowska M (2018) From isolation to connectivity: the effect of floodplain lake restoration on sediments as habitats for macroinvertebrate communities. Aquat Sci 80:4. https://doi.org/10.1007/s00027-017-0556-x
65. Osburn CL, Margolin AR, Guo L, Bianchi TS, Hansell DA (2019) Dissolved, colloidal, and particulate organic matter in the Gulf of Mexico. In: Bianchi TS (ed) Gulf of Mexico Origin, Waters, and Biota: Volume 5. Chemical Oceanography of the Gulf of Mexico. Texas A&M University, College Station, Texas, USA, pp 216–234
66. O'Shea TJ, Takeuchi NY, Weijs L, Marsh H (2018) Ecotoxicology of the Sirenia in the twenty-first century. In: Fossi MC, Panti C (eds) Marine mammal ecotoxicology: Impacts of multiple stressors on population health. Academic, London, pp 429–456. https://doi.org/10.1016/B978-0-12-804327-1.00016-4
67. Park J, Kumar M, Lane CR, Basu NB (2022) Seasonality of inundation in geographically isolated wetlands across the United States. Environ Res Lett 17:054005. https://doi.org/10.1088/1748-9326/ac6149
68. Poff NL, Olden JD, Merritt DM, Pepin DM (2007) Homogenization of regional river dynamics by dams and global biodiversity implications. Proc Natl Acad Sci USA 104:5732–5737. https://doi.org/10.1073/pnas.0609812104
69. Preiner S, Bondar-Kunze E, Pitzl B, Weigelhofer G, Hein T (2020) Effect of Hydrological Connectivity on the Phosphorus Buffering Capacity of an Urban Floodplain. Front Environ Sci 8:147. https://doi.org/10.3389/fenvs.2020.00147
70. Primost JE, Peluso L, Sasal MC, Bonetto CA (2022) Nutrient dynamics in the paraná river delta: relationship to the hydrologic regime and the floodplain wetlands. Limnologica 94:125970. https://doi.org/10.1016/j.limno.2022.125970
71. PROFEPA (2018) Reporte final: Atención de contingencia de manatíes en Tabasco. Procuraduría Federal de Protección al Ambiente, México.

https://www.gob.mx/cms/uploads/attachment/file/410558/Reporte_mortandad_de_manaties_act__05_nov_18.pdf. Accessed 30 Apr 2025

72. Qiao Q, Hao X, Yang C, Huang L (2025) Numerical and experimental investigation of hydrodynamics in an artificial chute cutoff under different hydrologic conditions. Discov Appl Sci 7:220. https://doi.org/10.1007/s42452-025-06677-z
73. Rendón-López MB, Suarez Alonso ML, Ayala-Ramirez GL, Hernández-Linares Y, Gómez-Tagle Chavez A, Medina-Avila JC, Vidal-Abarca MR (2016) Nutrients retention in a small subtropical wetland (México). J Limnol 75:17–30. https://doi.org/10.4081/jlimnol.2016.1363
74. Roach KA, Winemiller KO, Davis SE III (2014) Autochthonous production in shallow littoral zones of five floodplain rivers: effects of flow, turbidity and nutrients. Freshw Biol 59:1278–1293. https://doi.org/10.1111/fwb.12347
75. Romero J, García A, Bautista C, Pérez P (2000) Caracterización de la Reserva de la Biosfera Pantanos de Centla. Univ Cienc 15:15–28
76. Salcedo MA, Sanchez AJ, de la lanza G, Kampichler C, Florido R (2012) Condición ecológica del humedal tropical Pantanos de Centla. In: Sanchez AJ, Chiappa-Carrara X, Brito R (eds) Recursos acuáticos costeros del sureste. CONCIYTEY, Mérida, pp 112–136
77. Salcedo MA, Cruz-Ramírez AK, Sánchez AJ, Álvarez-Pliego N, Florido R, Ruiz-Carrera V, Morales-Cuetos SS (2022) Water Quality Indicators in Three Surface Hydraulic Connection Conditions in Tropical Floodplain Lakes. Water 14:3931. https://doi.org/10.3390/w14233931
78. Sánchez AJ, Álvarez-Pliego N, Espinosa-Pérez H, Florido R, Macossay-Cortez A, Barba E, Salcedo MA et al (2019) Species richness of urban and rural fish assemblages in the Grijalva Basin floodplain, southern Gulf of Mexico. Cybium 43:239–254. https://doi.org/10.26028/cybium/2019-433-005
79. Sánchez AJ, Florido R, Hernández-Trejo H, Álvarez-Pliego N, Salcedo MA, Barba E (2024) Ecological significance of a new record of *Vallisneria americana* Michx. in the conservation and sustainability of the Usumacinta Fluvial System. Discov Sustain 5:488. https://doi.org/10.1007/s43621-024-00748-8
80. Sánchez AJ, Florido R, Salcedo MA, Ruiz-Carrera V, Montalvo-Urgel H, Raz-Guzmán A (2012) Macrofaunistic diversity in *Vallisneria americana* Michx. in a tropical wetland, Southern Gulf of Mexico. In: Mahamane A (ed) Ecosystems I. InTech, Rijeka, pp 1–26
81. Sánchez AJ, Salcedo MA, Florido R, Armenta A, Rodríguez–Leal C, Galindo A, Moguel E (2007) Pantanos de Centla, un humedal costero tropical. In: De la Lanza G, Hernández-Pulido S (eds) Las aguas interiores de México, conceptos y casos. AGT Editores, México D.F., pp 399–422
82. Sánchez AJ, Salcedo MA, Florido R, Mendoza JD, Ruiz-Carrera V, Álvarez-Pliego N (2015) Ciclos de inundación y conservación de servicios ambientales en la cuenca baja de los ríos Grijalva-Usumacinta. ContactoS 97:5–14
83. Sandoval-Rivera JP, Sáenz-Arroyo A, Alcérreca-Huerta JC, Rodiles-Hernández R (2022) Impacto histórico de la deforestación y la modificación de los ríos en la morfología de la costa del sur del Golfo de México. Rev Hist (Concepción) 29:150–181. https://doi.org/10.29393/RH29-6IHJR40006
84. SAS Institute (2017) JMP statistics and graphics guide. Version 17. SAS Institute Inc, Cary
85. Savenko VS, Savenko AV (2022) The Main Features of Phosphorus Transport in World Rivers. Water 14:16. https://doi.org/10.3390/w14010016
86. Scott DW (2015) Multivariate density estimation: Theory, practice, and visualization, 2nd edn. Wiley, Hoboken. https://doi.org/10.1002/9781118575574
87. SEMARNAT (2000) Programa de manejo Reserva de la Biosfera Pantanos de Centla. Instituto Nacional de Ecología, Tlacopac, México, D.F. https://paot.mx. Accessed 15 June 2025

88. Serra-Llobet A, Jähnig SC, Geist J, Kondolf GM, Damm C, Scholz M, Lund J et al (2022) Restoring Rivers and Floodplains for Habitat and Flood Risk Reduction: Experiences in Multi-Benefit Floodplain Management From California and Germany. Front Environ Sci 9:778568. https://doi.org/10.3389/fenvs.2021.778568
89. Shen M, Liu X (2021) Assessing the effects of lateral hydrological connectivity alteration on freshwater ecosystems: A meta-analysis. Ecol Indic 125:107572. https://doi.org/10.1016/j.ecolind.2021.107572
90. Shuhaimi-Othman M, Lim EC, Mushrifah I (2007) Water Quality Changes in Chini Lake, Pahang, West Malaysia. Environ Monit Assess 131:279–292. https://doi.org/10.1007/s10661-006-9475-3
91. Soro MP, Yao KM, Kouassi NLB, Ouattara AA, Diaco T (2020) Modeling the Spatio-Temporal Evolution of Chlorophyll-a in Three Tropical Rivers Comoé, Bandama, and Bia Rivers (Côte d'Ivoire) by Artificial Neural Network. Wetlands 40:939–956. https://doi.org/10.1007/s13157-020-01284-7
92. Stevens C, Frost PC, Pearce NJT, Kelley JD, Zastepa A, Xenopoulos MA (2025) Limnological data derived from high frequency monitoring buoys are asynchronous in a large lake. PLoS ONE 20:e0314582. https://doi.org/10.1371/journal.pone.0314582
93. Thomaz SM, Bini LM, Bozelli RL (2007) Floods increase similarity among aquatic habitats in rivers-floodplain systems. Hydrobiologia 579:1–13. https://doi.org/10.1007/s10750-006-0285-y
94. Tian X, Wang H, Liang D, Zeng Y, Shen Y, Yan Y, Li S (2024) Water quality's responses to water energy variability of the Yangtze River. Water Sci Technol 89:635–652. https://doi.org/10.2166/wst.2024.008
95. Tockner K, Malard F, Ward V (2000) An extension of the flood pulse concept. Hydrol Process 14:2861–2883. https://doi.org/10.1002/1099-1085(200011/12)14:16/17%3C2861::AID-HYP124%3E3.0.CO;2-F
96. Tukey JW (1977) Exploratory data analysis. Addison-Wesley, Reading
97. Vero SE, Daly K, McDonald NT, Leach S, Sherriff SC, Mellander PE (2019) Sources and Mechanisms of Low-Flow River Phosphorus Elevations: A Repeated Synoptic Survey Approach. Water 11:1497. https://doi.org/10.3390/w11071497
98. Walalite T, Dekker SC, Schot PP, Kardel I, Okruszko T, Wassen MJ (2023) Nutrients in tropical and temperate rivers and floodplains – comparison of the Rivers Songkhram (Thailand) and Narew (Poland). Wetlands 43:46. https://doi.org/10.1007/s13157-023-01694-3
99. Wantzen KM, Junk WJ, Rothlaup KO (2008) An extension of the flood pulse concept (FPC) for lakes. Hydrobiologia 613:151–170. https://doi.org/10.1007/s10750-008-9480-3
100. Ward JV (1989) The Four-Dimensional Nature of Lotic Ecosystems. J N Am Benthol Soc 8:2–8. https://doi.org/10.2307/1467397
101. Weilhoefer CL, Yangdong P, Eppard S (2008) The effects of river floodwaters on floodplain wetland water quality and diatom assemblages. Wetlands 28:473–486. https://doi.org/10.1672/07-114.1
102. Wetzel RG (2001) Limnology: Lake and River Ecosystems, 3rd edn. Academic, San Diego. https://doi.org/10.1016/C2009-0-02112-6
103. Wohl E, Castro J, Cluer B, Merritts D, Powers P, Staab B, Thorne C (2021) Rediscovering, Reevaluating, and Restoring Lost River-Wetland Corridors. Front Earth Sci 9:653623. https://doi.org/10.3389/feart.2021.653623
104. Wu Z, Liu J, Huang J, Cai Y, Chen Y, Li K (2019) Do the key factors determining phytoplankton growth change with water level in China's largest freshwater lake? Ecol Indic 107:105675. https://doi.org/10.1016/j.ecolind.2019.105675
105. Zar JH (2010) Biostatistical analysis, 5th edn. Prentice Hall, Upper Saddle River
106. Zhang C, Chen L (2023) A review of wind-driven hydrodynamics in large shallow lakes: Importance, process-based modeling and perspectives. Camb Prisms Water 1:e16. https://doi.org/10.1017/wat.2023.14

107. Zhang Q (2025) Water Quality Assessment of River Basins: New Insights and Practical Solutions. Water 17:1207. https://doi.org/10.3390/w17081207

108. Zheng H, Tetzlaff D, Birkel C, Chmieleski J, Comte JC, Freymueller J, Goldhammer T et al (2025) Hydrological connectivity and biogeochemical dynamics in the function and management of the lower Oder floodplain. J Hydrol 653:132708. https://doi.org/10.1016/j.jhydrol.2025.132708

109. Zou W, Zhu G, Cai Y, Vilmi A, Xu H, Zhu M, Gong Z et al (2020) Relationships between nutrient, chlorophyll a and Secchi depth in lakes of the Chinese Eastern Plains ecoregion: Implications for eutrophication management. J Environ Manag 260:1–9. https://doi.org/10.1016/j.jenvman.2019.109923

Figures

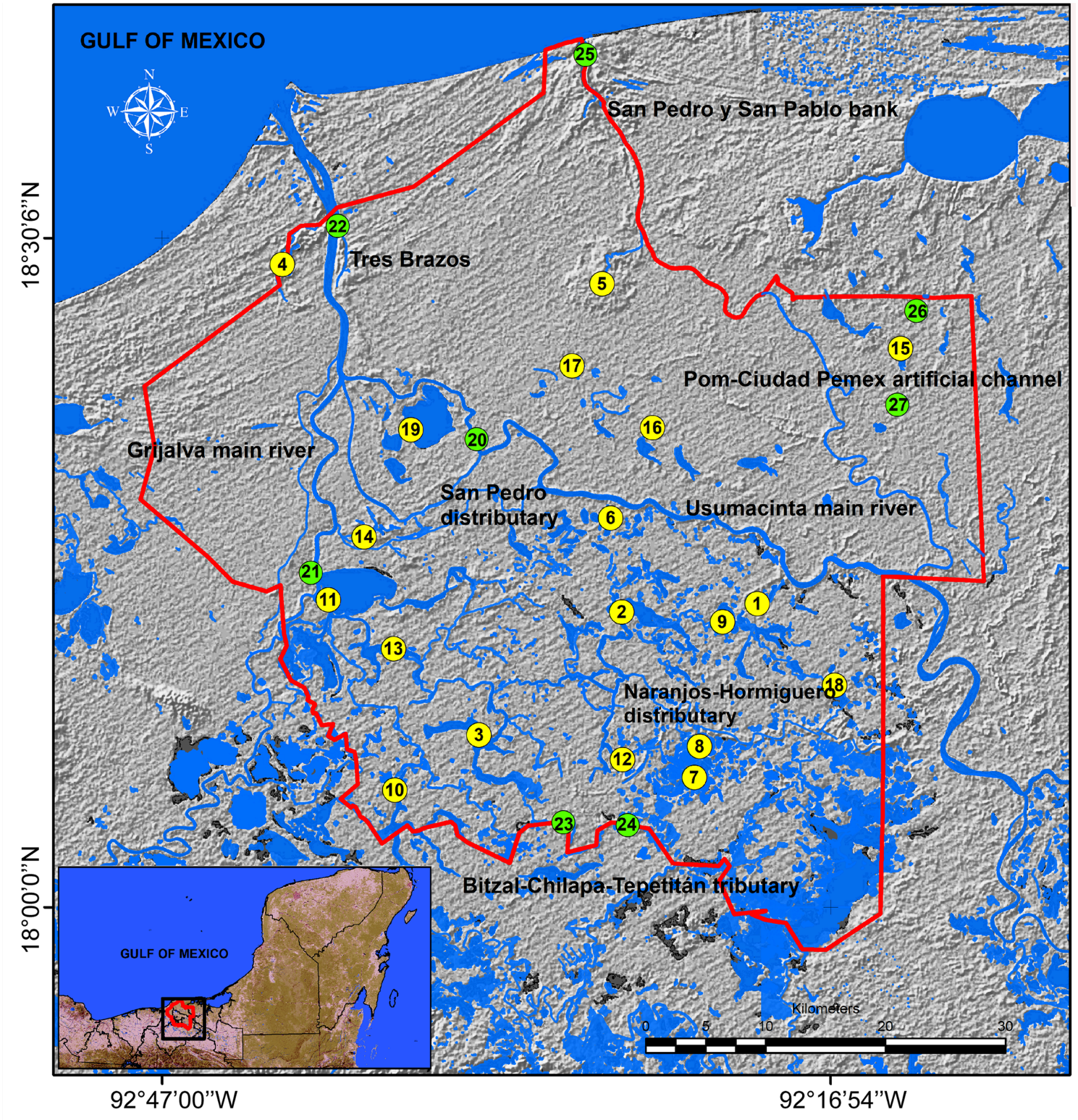


Figure 1

Sampling sites (n = 27) for the spatial and temporal analysis of the physicochemical and biological variables in Pantanos de Centla Biosphere Reserve (PCBR) in the Grijalva and Usumacinta fluvial systems. Red line = PCBR geographic borders, yellow circles = lentic sampling sites, green circles = lotic sampling sites https://goto.arcgisonline.com/maps/NatGeo_World_Map The base map is projected based on the WGS84 datum (Supplementary Table S1)

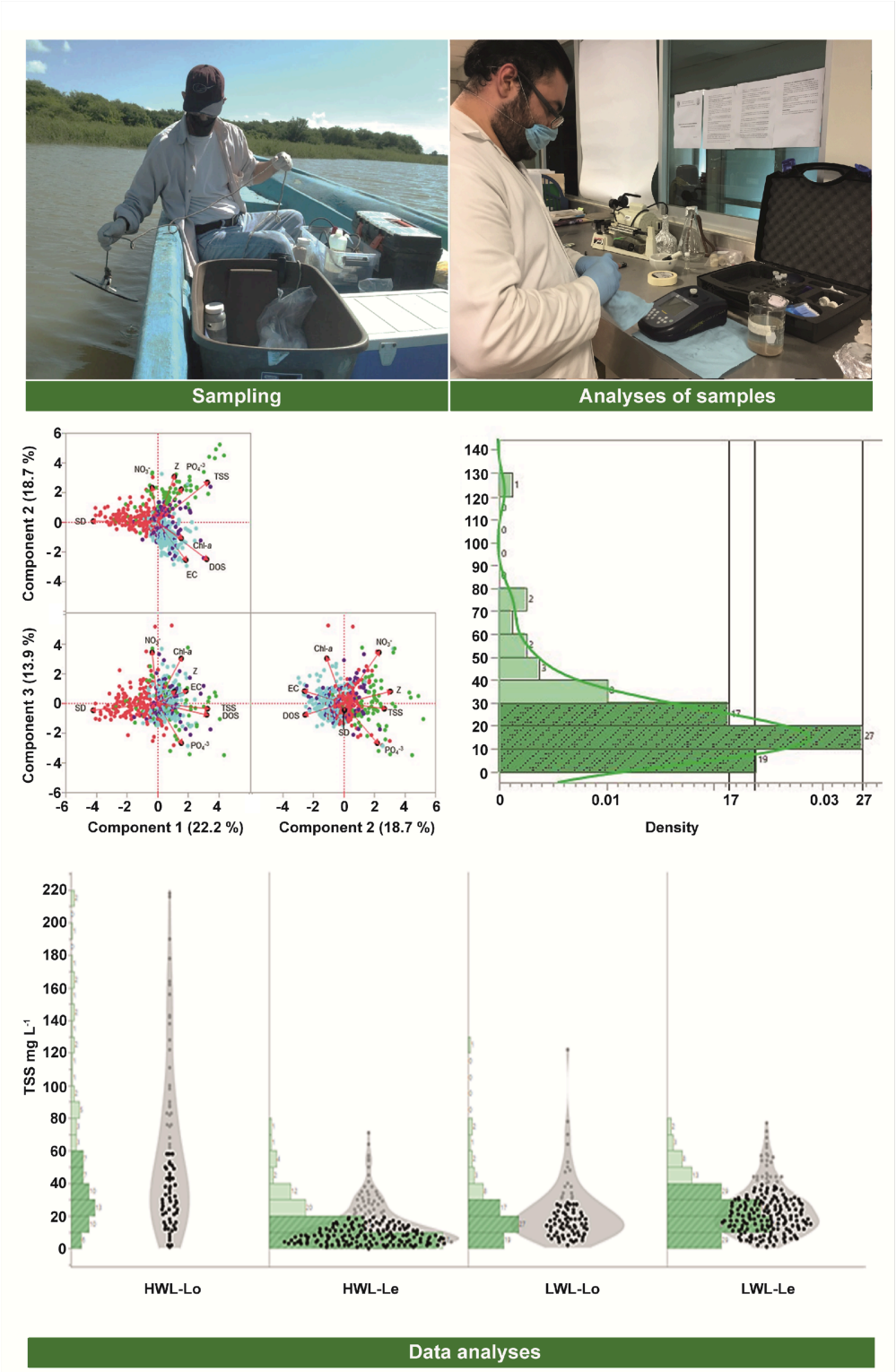


Figure 2

Sampling and data analysis of physicochemical and biological variables in Pantanos de Centla Biosphere Reserve in the Grijalva and Usumacinta fluvial systems

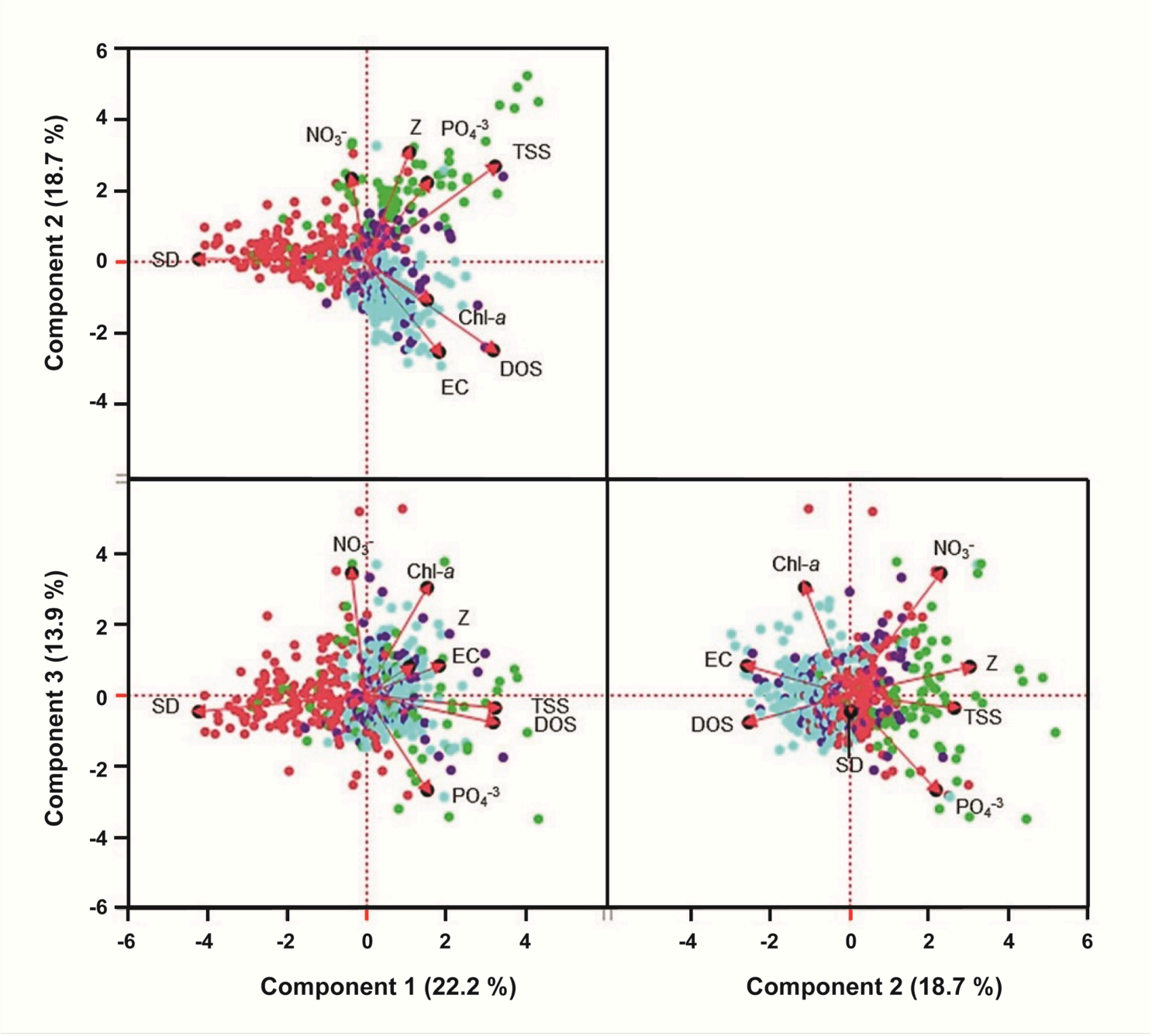


Figure 3

Spatial and temporal variation of eight key physicochemical and biological variables measured in lotic (Lo) and lentic (Le) ecosystems during low water level (LWL) and high water level (HWL) periods in Pantanos de Centla Biosphere Reserve in the Grijalva and Usumacinta fluvial systems. HWL-Lo = green dots, HWL-Le = red dots, LWL-Lo = purple dots, and LWL-Le = blue dots

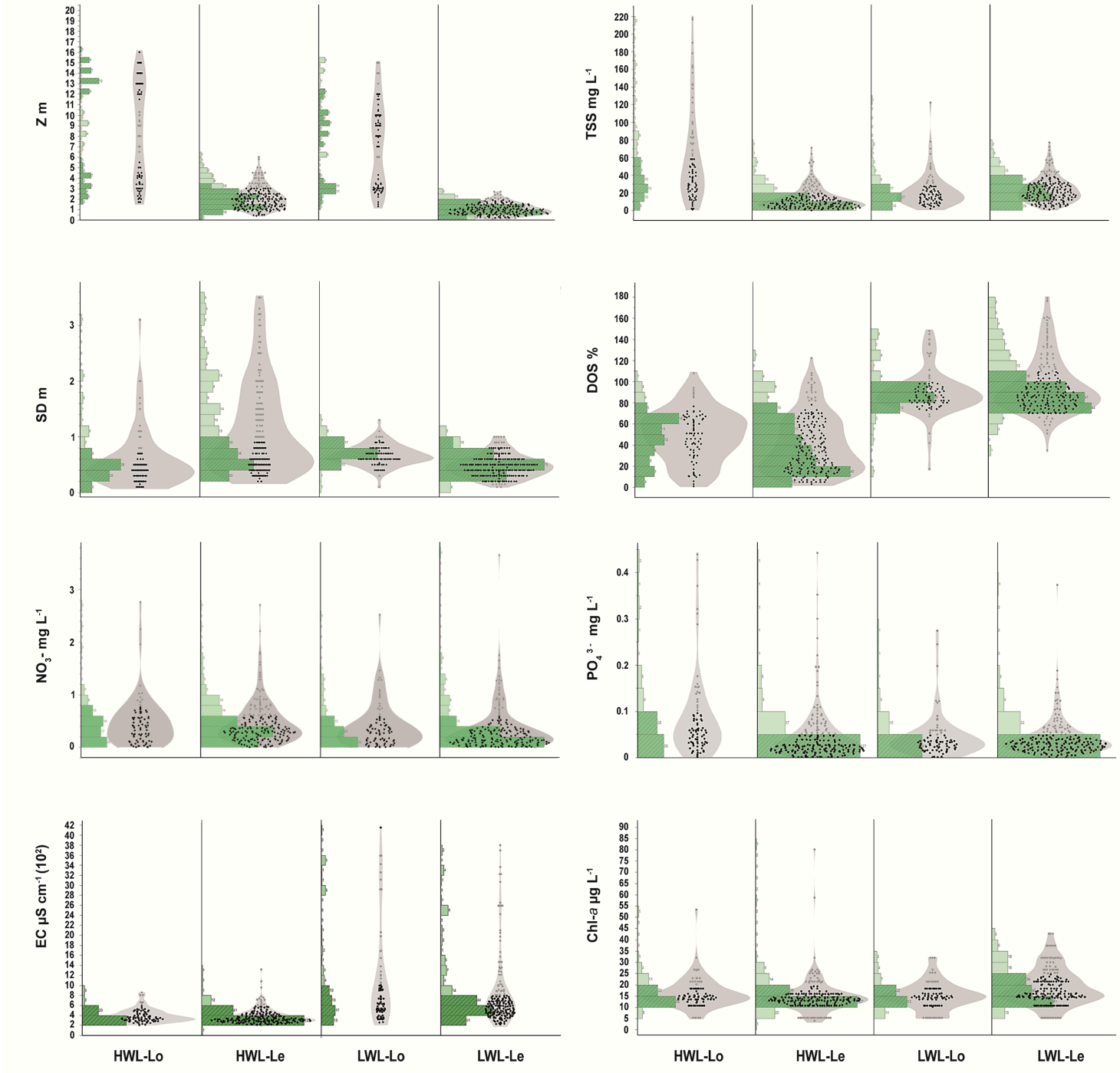


Figure 4

Description based on the data point distribution and interpretation of the spatial and temporal variation of physicochemical and biological variables in Pantanos de Centla Biosphere Reserve in Grijalva and Usumacinta fluvial systems. Green bins = data bump range, gray bins = data outside the bump, black dots = data points. Lotic (Lo) and lentic (Le) ecosystems during Low Water Level (LWL) and High Water Level (HWL) periods. Z = depth, TSS = total suspended solids, SD = Secchi disk depth, DOS = dissolved oxygen saturation, NO_3^- = nitrate, PO_4^{3-} = orthophosphate, EC = electrical conductivity, Chl-*a* = chlorophyll-*a*.